JOURNAL OF GEOPHYSICAL RESEARCH, VOL. 106, NO. C10, PAGES 22,095–22,113, OCTOBER 15, 2001

Zonal circulation in the NW Atlantic and Caribbean from a meridional World Ocean Circulation Experiment hydrographic section at 66°W

Terrence M. Joyce
Woods Hole Oceanographic Institution, Department of Physical Oceanography, Woods Hole, Massachusetts

Alonso Hernandez-Guerra
Universidad de Las Palmas de Gran Canaria, Departmento de Fisica, Las Palmas, Spain

William M. Smethie Jr.
Lamont Doherty Earth Observatory, Palisades, New York

Abstract. A World Ocean Circulation experiment Hydrographic Program section along 66°W in the North Atlantic was made in 1997. In addition to the usual variables (hydrographic and tracer) measured in WOCE onetime sections, we made lowered acoustic doppler current profiler (LADCP) measurements at nearly all of the stations. The section closed off a portion of the western North Atlantic to the west of the line, making a closed volume for constraining the circulation. In addition, the deep portions of the Caribbean do not communicate with the rest of the basin. By combining mass, silica, and LADCP information as constraints an inverse calculation obtained reveals a strong eastward transport in the Gulf Stream bounded by westward flowing water on either side. Within these energetic flows we see evidence for recently ventilated Classical Labrador Sea Water, which has not reached the Deep Western Boundary Current north of Puerto Rico in any significant amounts. Within the Caribbean our major new finding is a deep cyclonic circulation below sill depth in excess of 100 times the inflow of deep Atlantic water through the major deep sill: the Anegada-Jungfern Passage. The signature of the deep Atlantic source water is most prominent in CFCs and both a bottom and mid-depth maximum are present in the Caribbean to the south of Puerto Rico. Off the coast of Venezuela, however, only the deeper CFC maximum is found. For the entire section the net overturning circulation, heat flux, and freshwater fluxes are all consistent with expectations based on water mass formation and air-sea exchanges to the west of our section, but the annual mean air-sea fluxes of heat and freshwater from Comprehensive Ocean-Atmosphere Data Sets appear somewhat too small in comparison with our single-section result.

1. Introduction

This cruise was part of the World Ocean Circulation Experiment (WOCE) Hydrographic Program's (WHP) global, onetime survey of the oceans. The effort to study the global ocean with state of the art instrumentation for highest-quality measurements has been completed in all of the major ocean basins ending with the North Atlantic. As part of this effort, two meridional legs were planned for summer of 1997 aboard the R/V *Knorr* at 52° (WHP line designator A20) and 66°W (A22) as part of the U.S. Atlantic Circulation and Climate Experiment. These lines were done back to back beginning off the coast of Newfoundland, Canada, working southward along 52W to the coast of Suriname, with a port stop between legs in Trinidad. Our leg (Figure 1) worked northward from the coast of Venezuela to Puerto Rico and thence northwards (along 66°W) to the continental shelf south of Cape Cod, Massachusetts. Basic instrumentation and principal investigators for both meridional legs were the same with small changes in at-sea personnel. This report is for the second of the two meridonal legs (A22): the only WHP line in the global survey that sampled in the Caribbean Sea.

During the International Geophysical Year (IGY) in the mid-1950s and again in 1985, hydrographic stations were made to the ocean bottom in the region outside of the Caribbean along nominal longitudes of 66°W. Changes in water properties between these two occupations reflect long-term changes in the deep waters of the western North Atlantic [*Joyce and Robbins*, 1996]. Measurements made in 1997 along 66°W and 52°W were analyzed to document further the evolving system [*Joyce et al.* 1999], which is being strongly influenced by temporal changes in the Labrador Sea. Our efforts in this report will focus on the cruise data along 66°W in 1997; we present vertical sections of the basic hydrographic data including nutrients, clorofluorocarbons (CFCs), and lowered acoustic Doppler current profiler (LADCP) measurements in section 2. We discuss some of the water mass differences from the Caribbean to Atlantic proper and present a new multibeam bathymetric map of the

Paper number 2000JC000268.
0148-0227/01/2000JC000268$09.00

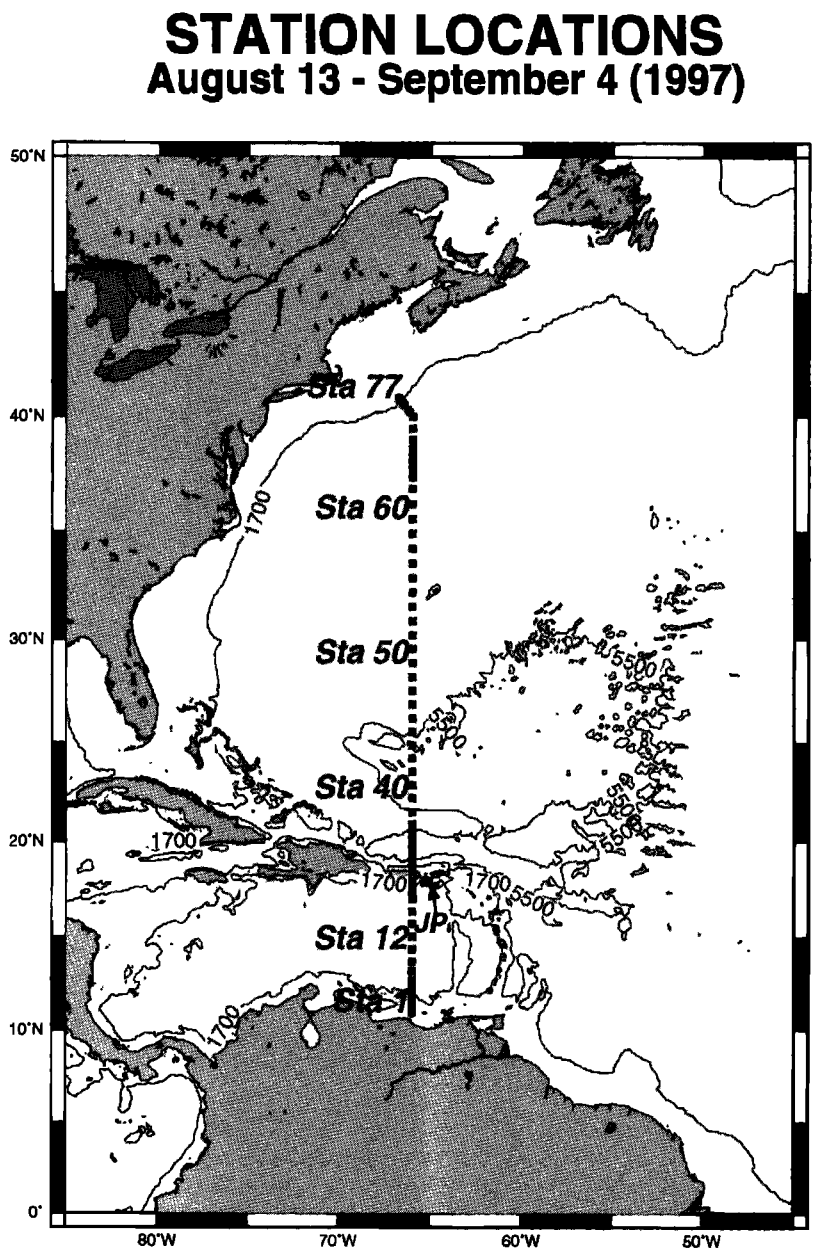

Figure 1. Station locations for the section. Also shown is the bottom bathymetry at 1700 and 5500 m depth and the approximate location of the Junfern Passage (JP), the deepest connection between the two portions of the section.

Jungfern Passage in section 3. We compare the LADCP and geostrophic velocity estimates and discuss how the two can be combined to provide absolute velocity profiles in section 4. We present the use of the LADCP data together with inverse model constraints on mass and silica fluxes is in section 5 followed by a discussion on the flow field and the meridional mass transport stream function for individual density layers and total mass in section 6. Finally, we consider the heat and freshwater balances implied by our circulation field in section 7.

2. Hydrographic Data and Vertical Sections

Station 1 was a test station made outside the Carioca Basin and stations 24 and 25 were in the Virgin Island Basin. The latter two are discussed in the next section. All others constitute the meridional section presented here: stations 2-23 in the Caribbean stations 26-77 in the North Atlantic proper. A cruise report and details of the individual measurement types made on the cruise are found in a WOCE cruise report for our section (A22), and the methodology follows that described in the WHP technical operations manual [*Joyce*, 1994]. A map (Figure 1) showing station locations indicates that distance intervals between stations varied depending on location: closely spaced stations over steep topography and the Gulf Stream and otherwise, station spacings of ~ 75 km. A 36 place, 10 L rosette was used for water sampling, and we show the bottle sampling plan (Figure 2a) and zonal current from the LADCP (Figure 2b) along with plots of potential temperature, salinity, neutral density [*Jacket and McDougall*, 1996], dissolved oxygen, nitrate, phosphate, silica, CFC-11 and CFC-12 (Plates 1a-1i). The LADCP data were collected

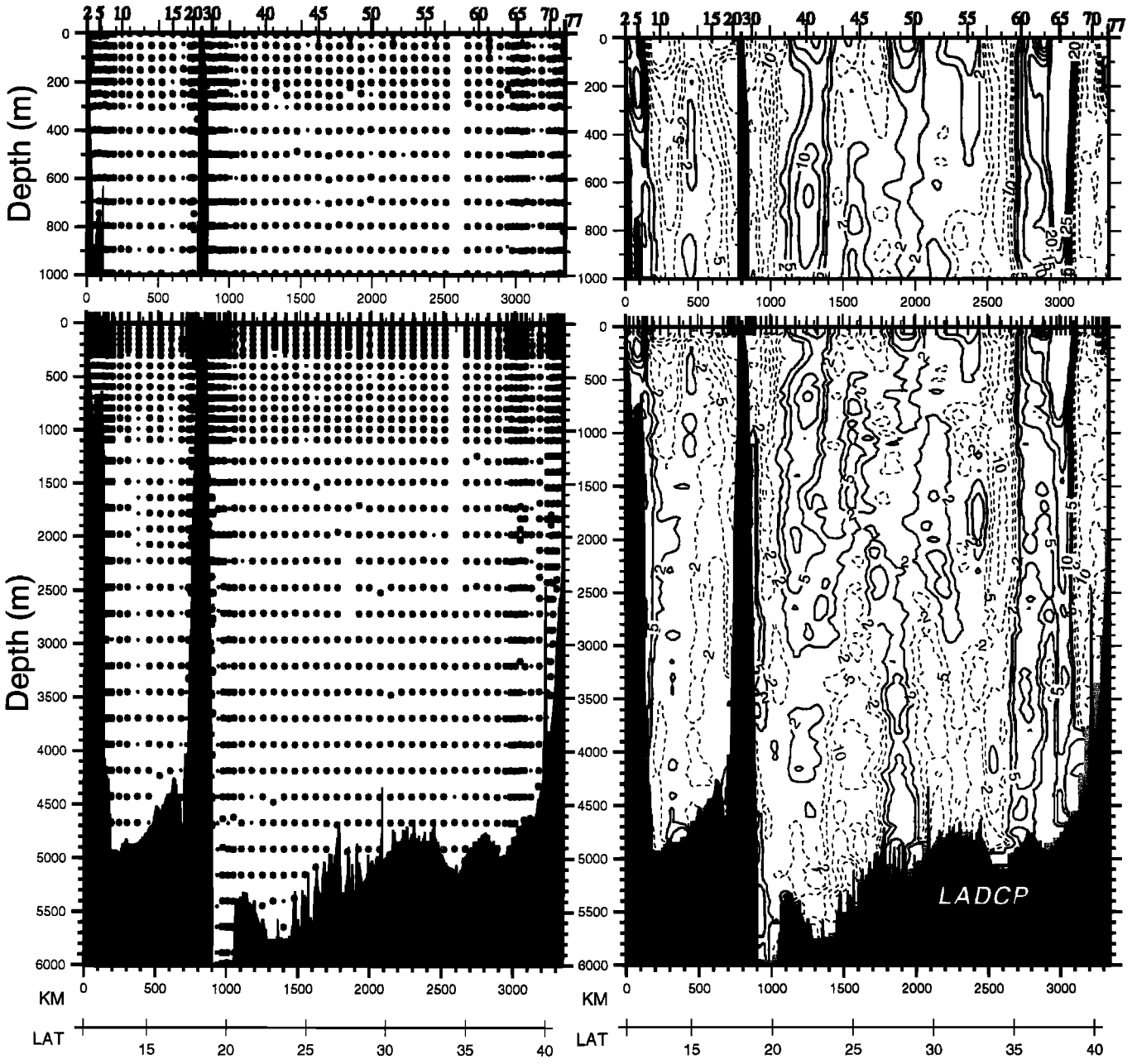

Figure 2. Section of bottle depths, with those at which CFCs were NOT sampled shown as the smaller dots. (a), LADCP currents normal to the section (b), solid (dashed) contours positive (negative).

with the conductivity-temperature-depth (CTD) package on each station as discussed later and combined with p code GPS navigation aboard the R/V *Knorr*. Because of instrument problems, no LADCP data were obtained on the upper slope south of Puerto Rico (stations 20-23). For clarity we have not plotted bottle locations on the bottle-derived sections but have shown our sampling scheme separately.

Our section crossed the Deep Western Boundary Current (DWBC) twice: once to the north of Puerto Rico and a second time off the continental slope south of New England. The Gulf Stream crossing (stations 64-68) is characterized by steeply sloping isopycnals (Plate 1c) and strong eastward flow (Figure 2b) all the way to the ocean bottom. North of the Gulf Stream, the flow is westward at all depths, and we see evidence for the DWBC in the salinity, oxygen, nutrients, and CFCs, with a suggestion of two tracer cores at depths of roughly 1500 and 3000 m depth. This DWBC signature is seen again near Puerto Rico at depths of 1500 and 3500 m, although this is more attenuated in the tracers. The high-CFC and high-oxygen signals in the deep waters are due to a mixture of Iceland-Scotland and Denmark Strait overflow waters with Denmark Strait Overflow Water providing most of the CFC signal [*Smethie*, 1993, *Smethie et al.*, 2000], while those at mid depths come from the Labrador Sea. To the north of Puerto Rico this latter maximum is at the depth and potential temperature of Upper Labrador Sea Water (ULSW), [*Pickart*, 1992; *Smethie*, 1993; *Smethie et al.*, 2000] and not classical Labrador Sea Water (CLSW), which was formed in relatively small amounts from 1977 to 1988 and relatively large amounts from 1988 to the mid-1990s [*Lazier*, 1995]. At

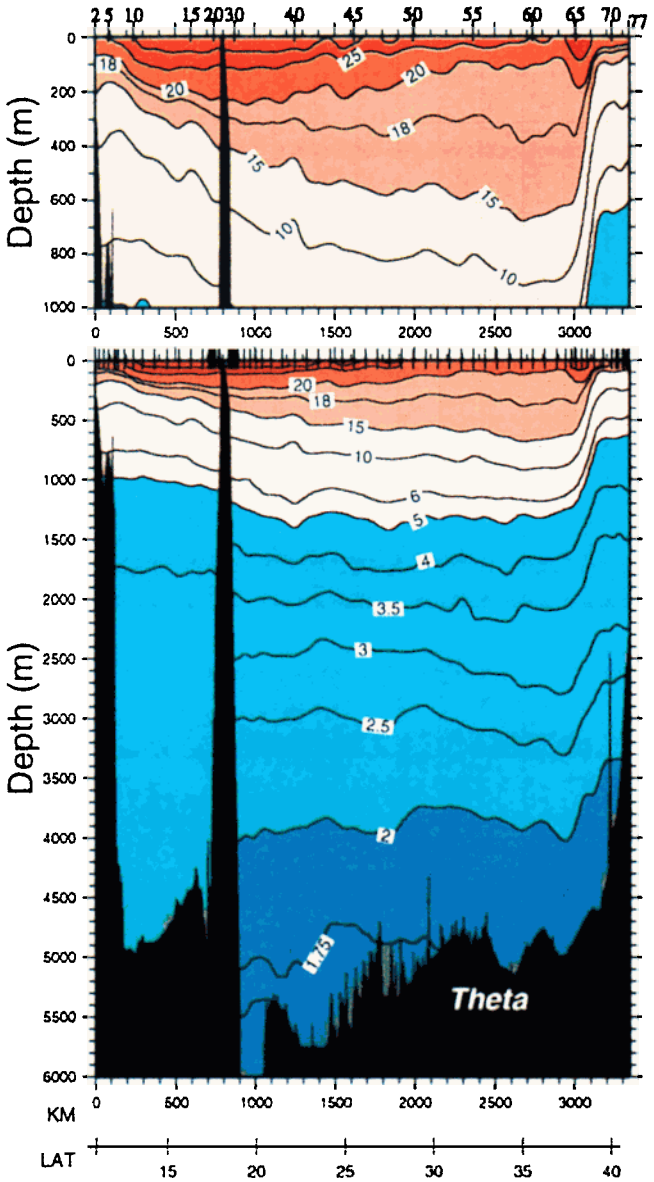

Plate 1a. Potential temperature (°C).

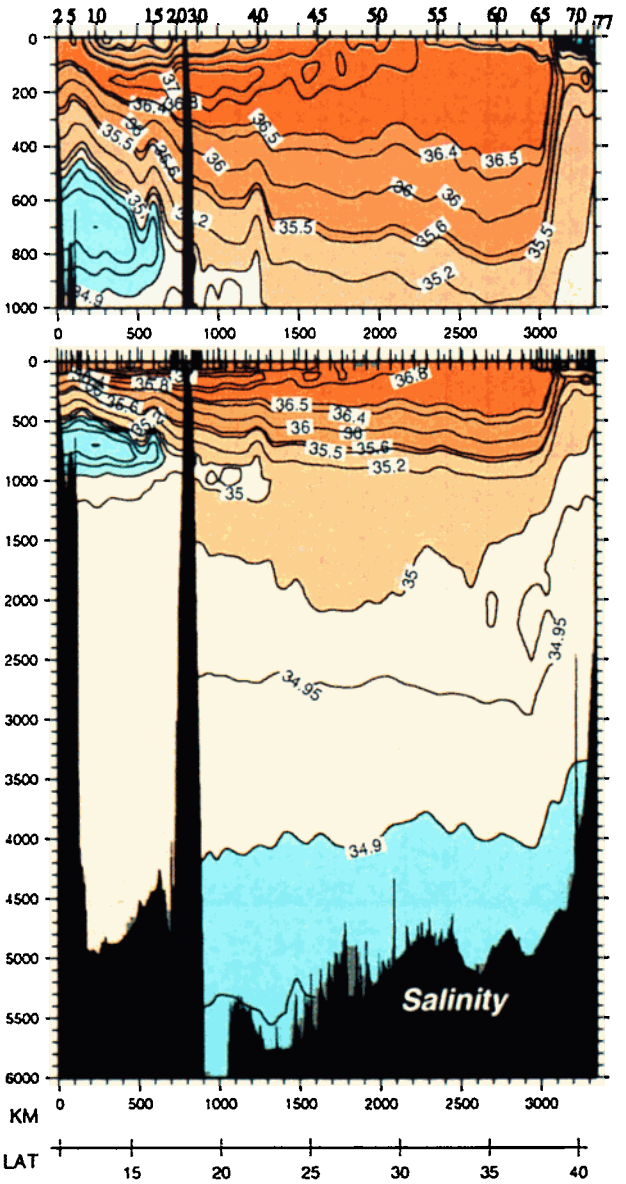

Plate 1b. Salinity.

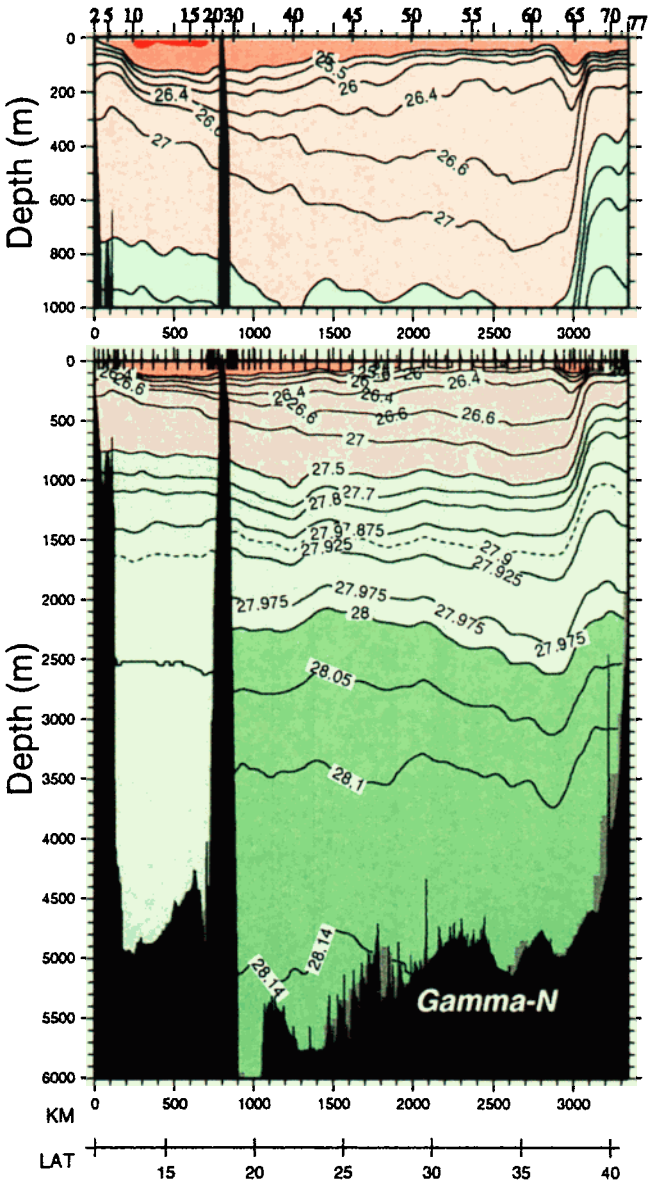

Plate 1c. Neutral density (kg m^{-3}).

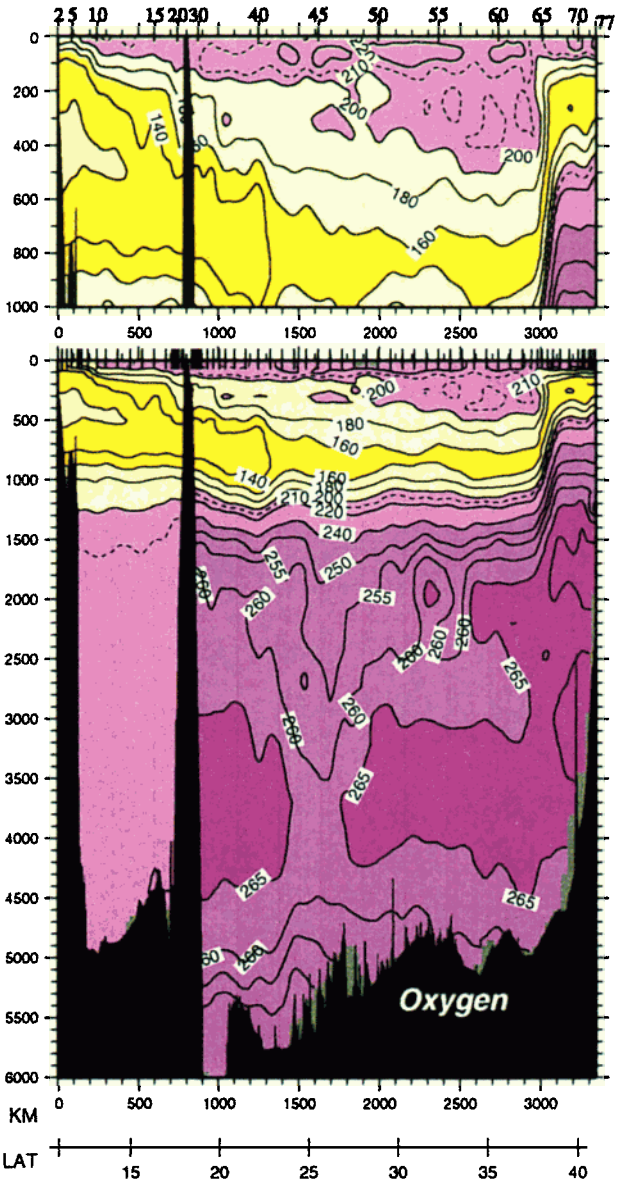

Plate 1d. Dissolved oxygen (μmole kg^{-1}).

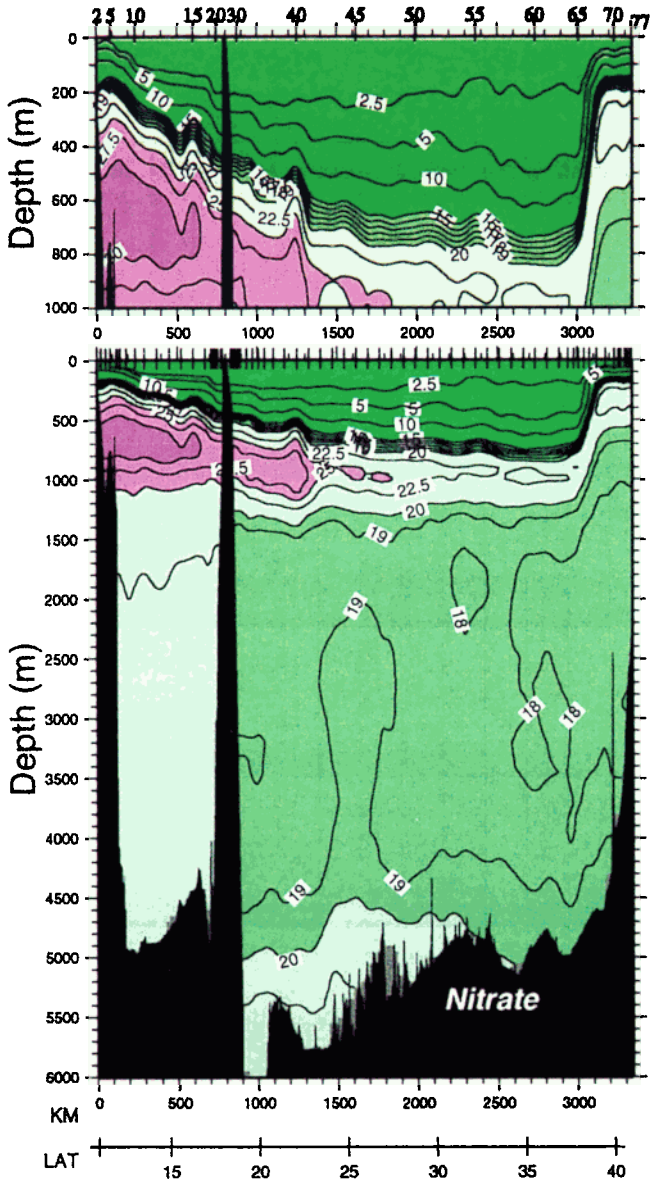

Plate 1e. Nitrate (μmole kg^{-1}).

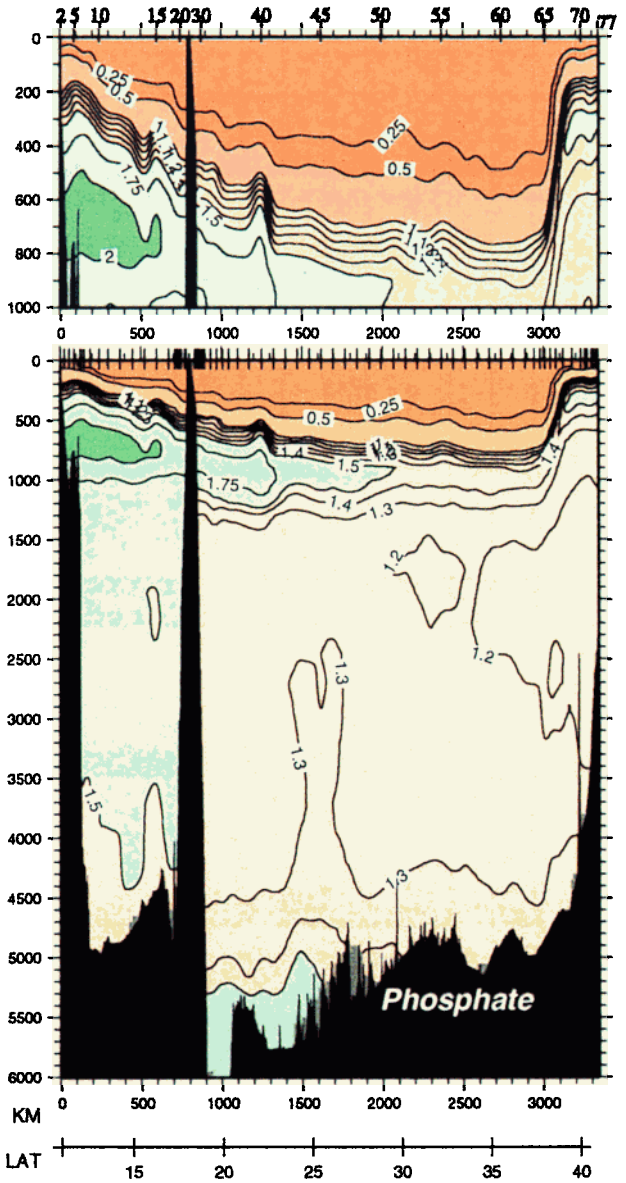

Plate 1f. Phosphate (μmole kg^{-1}).

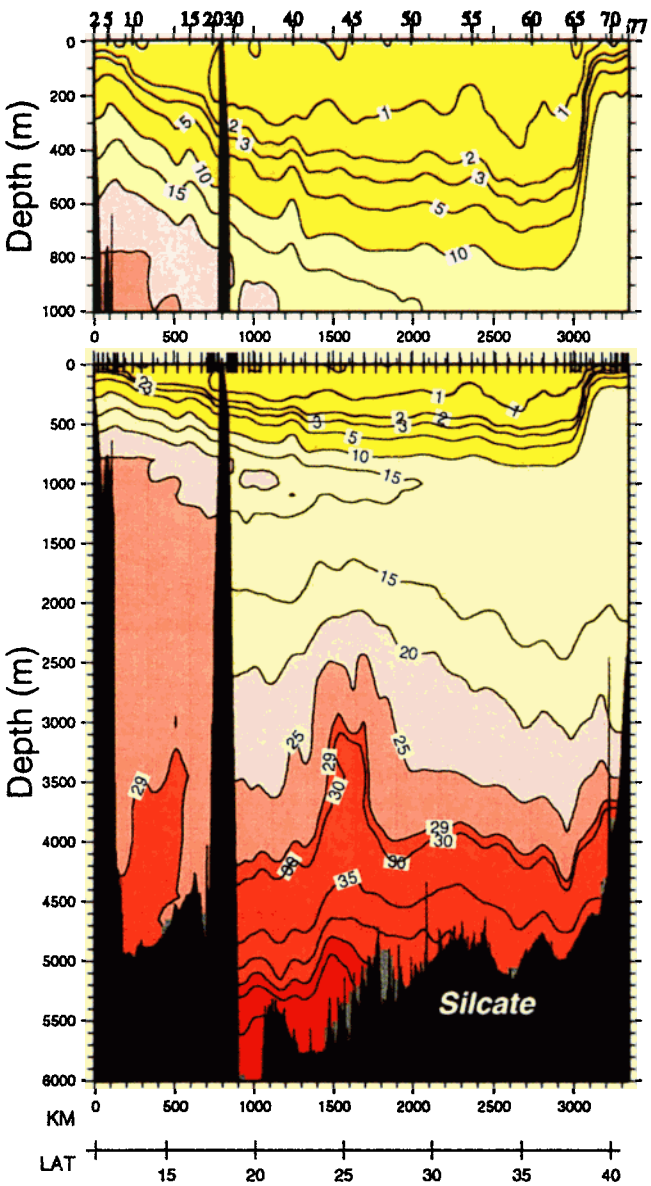

Plate 1g. Silica (μmole kg^{-1}).

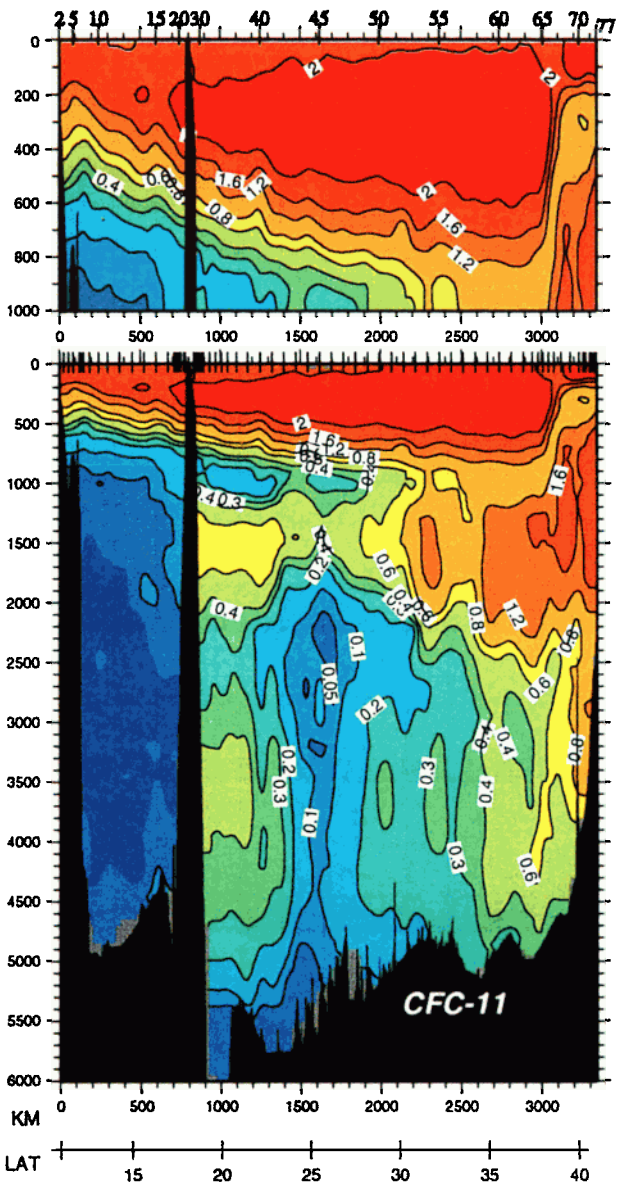

Plate 1h. CFC-11 (pmol kg^{-1}).

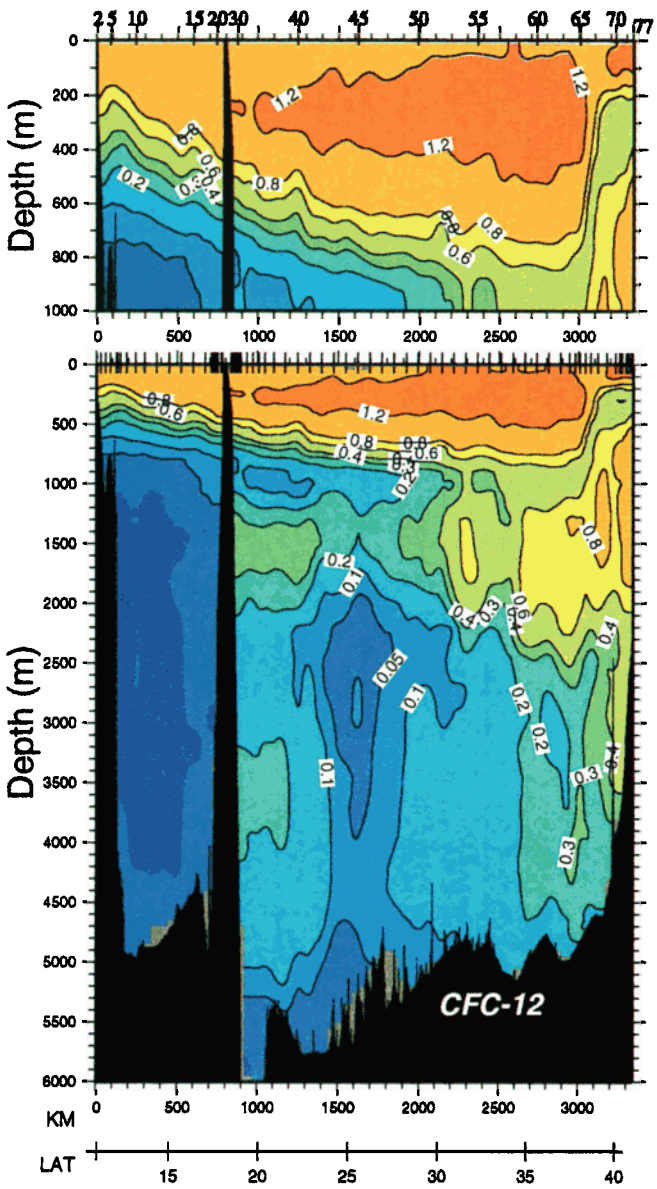

Plate 1i. CFC-12 (pmol kg^{-1}).

the time of our section, CLSW was not yet present in large amounts near Puerto Rico [see also *Joyce et al.*, 1999], but was present in large quantity at the northern boundary of our section, where the mid depth tracer extremum is at a higher density and lower potential temperature (corresponding to CLSW) than the one to the north of Puerto Rico. Previously, this recently renewed water mass was observed south of the Grand Banks by *Pickart and Smethie* [1998] and *Smethie et al.* [2000]. To the north of Puerto Rico the eastward flowing DWBC is evident in the LADCP section, which also shows a reversal and continuation of the eastward flow to about 23°N. In general, the tracers (oxygen, nutrients, and CFCs) portray a well-ventilated North Atlantic basin with high oxygen and CFCs and low nutrients everywhere except in a narrow band between about 24° and 27°N.

This high degree of ventilation contrasts markedly with the Caribbean which has no connection to the North Atlantic deeper than about 1700 m depth other than that located in the Anegada-Jungfern (A-J) Passage east of Puerto Rico. We will come back to this connection and the implications on the deep structure of the Caribbean later. For now note the relative low in silica and high in CFCs near the bottom periphery, low CFCs at mid basin, and the suggestion of a middepth extremum in the CFCs at about 2000 m depth just to the south of Puerto Rico. These suggest that what North Atlantic water is entering can occasionally reach the bottom, but is found preferentially on the edge of the basin. This deepest entering N. Atlantic water is from the Labrador Sea with a density between that of ULSW and CLSW, and it is mixed with ambient Caribbean water after entering the basin. The mixture still retains the high-oxygen, high-CFC and low-nutrient signature of its Labrador Sea origins. The oxygen, silica, and CFC-11 contrasts between the deep water on the northern rim of the Caribbean and the interior are 3 μmole kg^{-1}, -2 μmole kg^{-1}, and 0.03 pmole kg^{-1}, respectively. At the northern end of the section in the Caribbean the LADCP data indicate a concentrated westward flow in the deep water, with a similar concentrated eastward flow at the southern boundary of the basin. This evidence for a cyclonic rim current in the Caribbean will be further discussed after our inverse solution in section 6.

The upper layers of the Caribbean show the westward flowing low-salinity Antarctic Intermediate Water (AAIW) (600-900 m) with a salinity signal that can be traced to the north of Puerto Rico with decreasing amplitude and increasing depth. A similar trend can be found for the low-oxygen Tropical Atlantic Central Water (300-600 m) located just above the AAIW layer. Both of these water masses were identified in that basin by *Wüst* [1964], although it was *Metcalf* [1976] who labeled the oxygen minimum layer with a water mass originating from the tropical Atlantic. Both of these water masses are found in our section most clearly on the southern side of the Caribbean with diminished minima extending into the southern edge of the Saragasso Sea. While the flow field at 66°W indicates a generally westward current in the Caribbean, there is clear evidence for an eastward, upwind flow near the Venezuelan coast and slope. A further discussion of the upper layer properties and flow field in the Caribbean is presented by *Hernandez-Guerra and Joyce* [2000].

A subsurface salinity maximum (S > 37) can be seen to the north of Puerto Rico and extending into the northern part of the Caribbean at a depths of about 150 m. This Subtropical Underwater (SUW) was also identified in the Caribbean by *Wüst* [1964], who attributed its origin to be in the high evaporation regions of the subtropics. One can also see a clear signature of 18° [*Worthington,* 1959] Subtropical Mode Water (STMW) in all of the hydrographic property fields, particularly potential temperature and CFCs, most prominent to the south of the Gulf Stream and narrowing, nearly linearly, in thickness with decreasing latitude toward Puerto Rico. *Metcalf* [1976] discussed the inflow of this water mass into the Caribbean through the A-J Passage, to which we will now turn our attention.

3. Virgin Island Basin and Jungfern Passage Bathymetry

Stalcup and Metcalf [1973] published some updated bathymetry of the deepest passage from the Atlantic into the Caribbean. This has been augmented by a recent study of

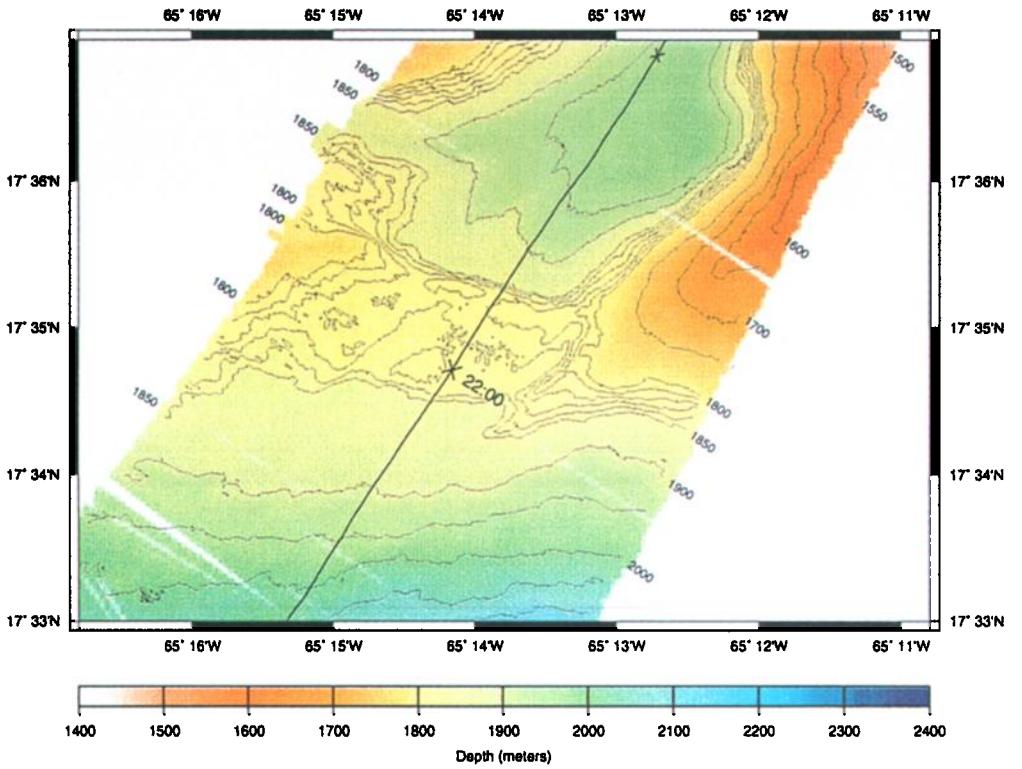

Plate 2. Multi-beam bathymetry of the Jungfern Passage (depth in corrected meters).

Fratantoni et al. [1997]. Going from the Atlantic side into the Caribbean, this passage begins with the Anegada Passage with a sill depth of 1915 m moves into the Virgin Island Basin (VIB) with depths in excess of 4000 m and thence moves through the Jungfern Passage (JP) with a maximum sill depth of 1815 m. A secondary passage, the Grappler Channel (GC), has a maximum sill depth of 1710 m. Since the *Knorr* had to transit between the Caribbean and the Atlantic as it rounded Puerto Rico, we chose to occupy a pair of stations in the VIB. During the transit the multi-beam SeaBeam™ system produced a detailed bathymetric map of the JP (Plate 2) which we have corrected using the sound speed derived from a CTD cast from the *Endeavor* 129 cruise in 1985 [*Knapp*, 1988, station 7], while also correcting for the transducer depth on the ship. This map indicates the maximum sill depth in the JP within a narrow channel of depth 1824 m, with a broad saddle point at a depth of about 1820 m. We show this map because we are not aware of any previous multi-beam bathymetry from this important deep water passage. *Metcalf* [1976] noted that waters in the VIB had Atlantic characteristics from the surface down to depths of 700 m, below which, Caribbean waters occupied a more prominent role to a depth of 1200 m. At deeper depths the Atlantic character becomes more prominent again, especially below a potential temperature of 4°C. Thus we see that the A-J Passages offer an exchange route by which the two portions of our section can communicate.

Time series measurements of the deep inflow in the JP and GC were made over a period of about 14 months by *MacCready et al.* [1999]. They find a net inflow of Atlantic water with $\theta < 3.965$°C of about 0.11 ± 0.05 Sv. As the inflowing water is colder and saltier than the Caribbean water at the same depth, dense overflow plumes form that can reach depths from 2000 m to the bottom of the Caribbean, according to the *MacCready et al.* [1999] application of the *Price and Baringer* [1994] plume model. Our tracer section in the Caribbean indicates on the basis of the oxygen, silica, and CFC measurements that both a mid depth and a bottom injection have occurred . We will return to the interpretation of our measurements in terms of the plume results later.

4. LADCP Measurements and Geostrophic Reference Velocity

A 150 kHz LADCP was used and absolute velocity data estimated using the techniques described by *Firing and Gordon* [1990] as further documented by *Fischer and Visbeck* [1993]. In order to compare the LADCP-derived velocities with those determined geostrophically using the CTD data from neighboring stations we averaged the LADCP data from the two adjacent stations and compared those averages with the average geostrophic flow between the two stations. It is expected that small-scale velocities due to unresolved geostrophic currents may contribute to the LADCP endpoint averages but not to the average from a CTD station pair. It is further anticipated that actual LADCP velocities may not be geostrophic, especially near the surface. Thus we do not, in general, expect an exact agreement between the two velocity fields. We seek from each station pair a constant velocity offset to be added to the geostrophic estimate in order to minimize the difference between the two different velocity profiles over a given depth interval. We have chosen to make this determination on the basis of visual inspection of various station pairs, usually selecting a substantial depth interval (order 1 km) in the deep water for the matching. As noted above, this was not possible for all station pairs either because

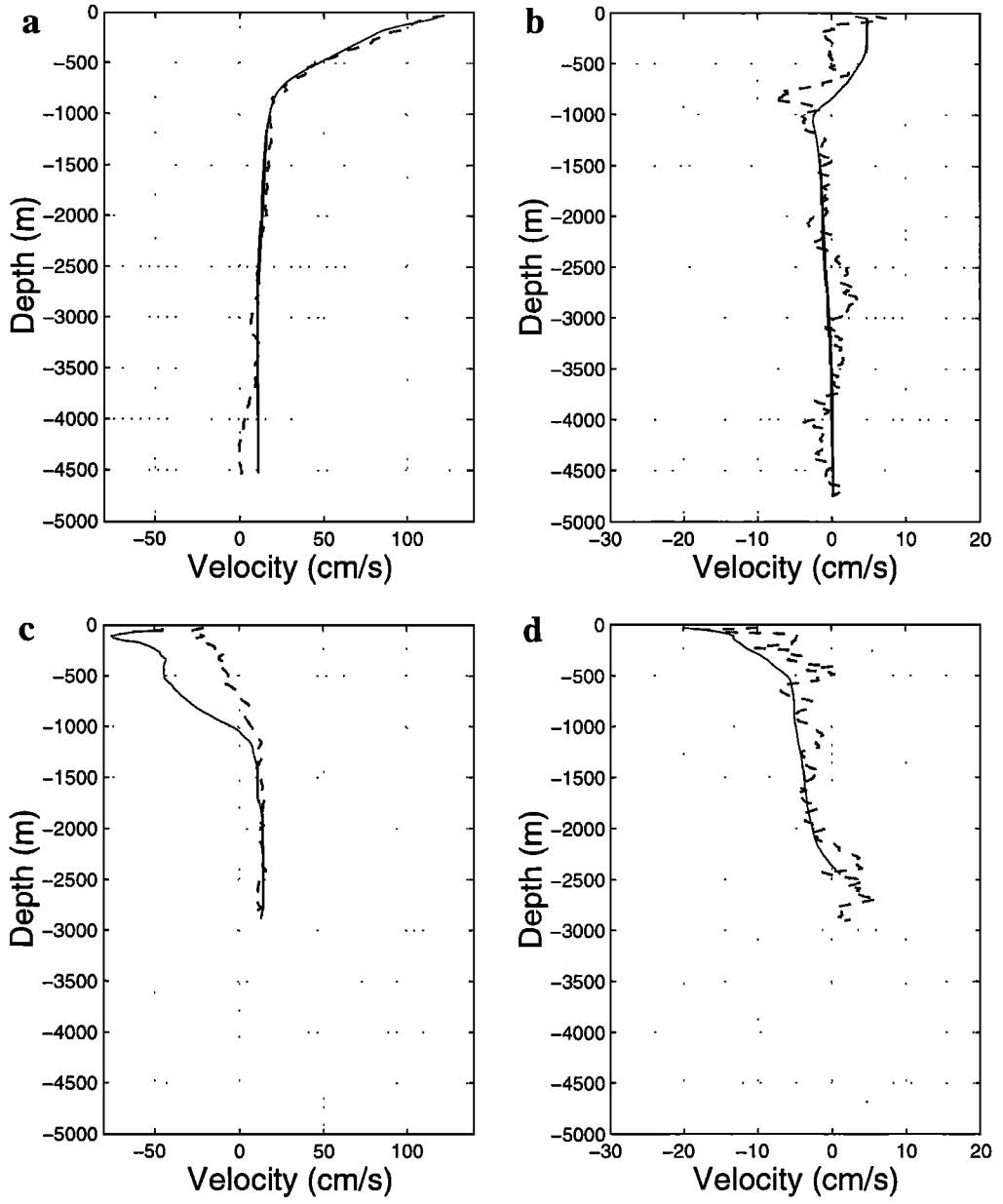

Figure 3. Selected comparison between geostrophic and LADCP currents: (a) Gulf Stream, stations 67-68; (b) Sargasso Sea, stations 54-55; (c) DWBC, stations 31-32; and (d) DWBC, stations, 72-73. In all cases, the reference velocity for the geostrophic flow has been added on the basis of our fit to the two different estimates. Note the scale change between Figures 4a and Figures 4b and 4d. LADCP data are dashed lines; adjusted CTD data are solid lines.

of lack of LADCP data (some stations south of Puerto Rico) or because of excessively noisy LADCP/CTD-derived comparisons in shallow water. In the latter we expect ageostrophic effects to be large. In both cases we chose to make no estimate of the reference velocity. For the above any initial reference level can be chosen for the CTD data, and for simplicity we chose a level of no motion at the depth of the 27.9 neutral density level. The initial velocity field with this reference level is discussed in section 5 along with various mass imbalances. For now, let it be stated that the above fitting procedure altered the velocity field substantially, but did not eliminate the need for further (inverse) constraints on the absolute flow.

We show several examples (Figure 3) from various portions of our section including the DWBC south of New England and north of Puerto Rico, the Gulf Stream, and finally, the Sargasso Sea. The lower 800 m of the Gulf Stream pair and the upper 1000 m of the DWBC pair north of Puerto Rico both show the nature of the differences between the two estimates. In the former (Figure 3a, upper left panel) we expect that near-bottom topography and/or high-frequency internal/inertial waves might be important in explaining the differences near the bottom. In the latter (Figure 3c), the small-scale, even frontal nature of the westward flow north of the island is most likely poorly resolved by taking the average of two LADCP profiles as representative of the average flow

between stations. In Figures 3b and 3d, the differences have an oscillatory character most likely due to high frequency, ageostrophic motions. In the vertical interval over which we do the fit for each station pair we can obtain the residual error, which is one estimate of the error in the determination. However, the above mentioned areas over which we did not fit also represent to a degree the "error" in the geostrophic reference. In general, we have simply ascribed a fixed error of ± 5 cm s^{-1} to every reference velocity.

Table 1. Neutral Density Levels Used in Analysis

γ_n	Layer	Water Mass
20		
	1	surface layer
25		
	2	upper thermocline
25.5		
	3	SUW
26		
	4	upper thermocline
26.4		
	5	STMW
26.6		
	6	lower thermocline
27		
	7	AAIW
27.5		
	8	AAIW
27.7		
	9	AAIW
27.8		
	10	ULSW
27.875		
	11	LSW
27.925		
	12	CLSW
27.975		
	13	ISOW
28		
	14	ISOW
28.05		
	15	DSOW
28.1		
	16	LDW
28.14		
	17	AABW
29		

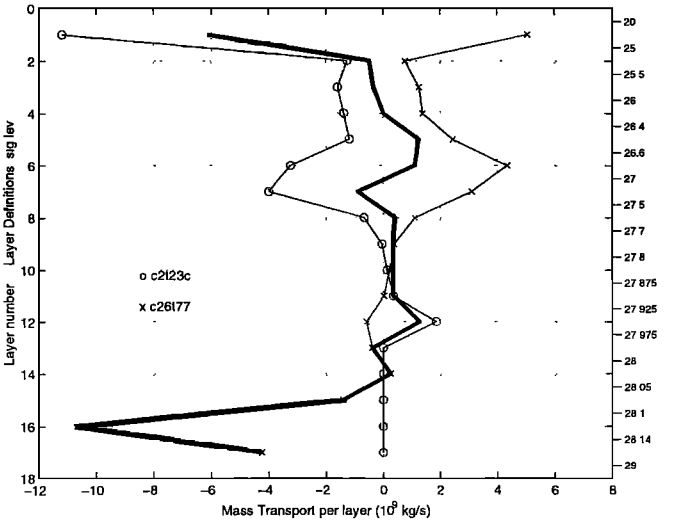

Figure 4. Meridionally integrated mass flux as a function of density layer for the Caribbean (circles) and Atlantic (crosses) portions of our section, together with their sum (heavy solid line).

5. Inverse Calculation

5.1. Initial Reference Level Circulation

Initially, we used a reference level of no motion at the 27.9 neutral density level. This level, shown as a dashed line in the density section (Plate 1c), though being part of the ULSW, lies near the reversal in the mean transport across the section, as we will see after all of the following absolute velocity calculations. If one or both stations of each station pair was shallower than this level, the deepest common level was used as the velocity reference. Bottom triangle transports were calculated using the deepest common level velocity extended without change to the bottom. Actual bathymetry was used between stations rather than just at station locations.

We have divided up the water column into a number of layers on the basis of neutral density (Table 1), which are roughly defined as water mass boundaries. The Caribbean Sea consists of three major basins: Venezuelan, Colombian, and Yucatan. The latter two are isolated below 1500 m from one another, and thus our section is closed off to the west at depths below 1500 m. Furthermore, since there is no major flow through the Panama Canal, our entire section is closed off to the west. Thus we can reasonably impose the following constraints based on density levels: no net transport in layers 11–12 in the Caribbean, no net mass transport in layers 11–17 north of the Caribbean, and no net mass transport in layers 1-17 for the entire section. Our section, which runs north/south, is nearly perpendicular to the mean winds. We have used the wind stress estimates from NSCAT/ERS-1 for the period 1991–1998 [*WOCE,* 1998] to calculate Ekman transports across our section. They are small in both the Caribbean (-.18 Sv, 1 Sv = 10^9 kg s^{-1}) and the Atlantic (0.09 Sv) portions of our sections. Therefore, to a large degree the above statements about mass conservation apply to the geostrophic circulation.

If the initial level at 27.9 is used for geostrophy, we obtain basin-wide mass transports (Figure 4) in each subbasin of our section that mirror one another, with a net westward inflow in the upper layers into the Caribbean and a net eastward outflow to the north, mainly in the region of the Gulf Stream.

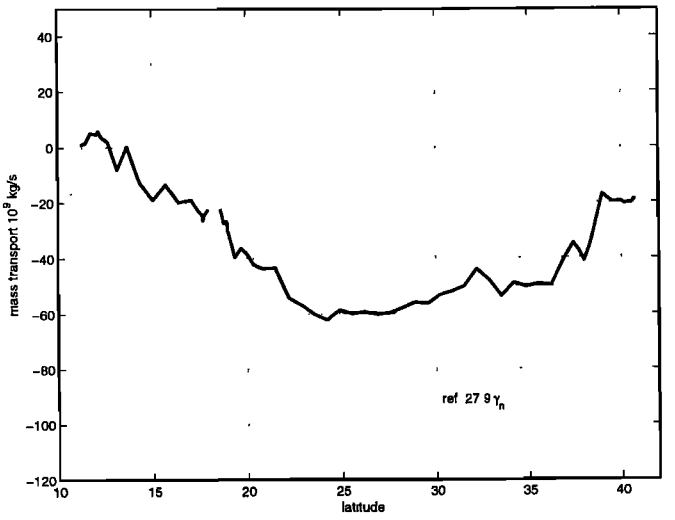

Figure 5. Vertically and meridionally integrated mass transport stream function for the geostrophic circulation using a zero velocity level at a neutral density of 27.9. The integration was begun at the coast of Venezuela. The break in the stream function is at the island of Puerto Rico.

The initial layer integrated stream function (Figure 5) shows a net transport of -22 Sv into the Caribbean and a net transport of only 3 Sv out of the northern subbasin. Clearly, there is a problem with this initial reference layer: while the layer transports nearly balance in the upper ocean, the above constraints are clearly violated. We see that there are large imbalances in the deep water to the north, with a large inflow of deep water of Denmark Straits, Antarctic Bottom Water, and Lower Deep Water [*McCartney*, 1992] origin.

5.2. Initial LADCP-Derived Reference Level Circulation

Using the LADCP to provide a reference for the geostrophic velocity, a revised reference velocity was chosen, and this subsequently led to a revised zonal circulation pattern. The subbasin integrated results (Figure 6) mask the fact that the flow is substantially larger, especially in the region of the Gulf Stream, its recirculation regime, and the DWBC. We can see that the deep inflow of Figure 4 has been reduced, but the LSW at shallower depths now has a net mass loss from the section. It is this mass imbalance which will be used to modify the circulation using an inverse solution.

5.3. Mass Constraints

Mass, salt, and nutrient transports for each layer and for each station pair were calculated using the thermal wind equation with a reference velocity other than zero and different for each station pair. This velocity was obtained from the LADCP data as already described. We also considered and included the Ekman transport in the first layer of mass, salt and nutrient transports. Our initial equations for the inverse calculation [*Wunsch*, 1978], formulated in a matrix form, are as follows:

$$Ab+n=-\Gamma, \tag{1}$$

where A is an $m \times n$ matrix, with elements A_{ij} equal to the product of the area, density, and concentration of property (e.g., mass) of constraint i at station pair j; b a column vector, with elements b_j the unknown, new reference velocity for each station pair; n is an m column vector, with elements the noise of each constraint; and Γ is a column vector, with elements equal to the property imbalance resulting from the relative velocity plus the adjusted LADCP velocity.

Our initial requirement was that mass be conserved not only in each layer (Table 1), but overall, to within some a prioi estimate of error. Specifically, our inverse problem consisted of 72 unknowns, the new reference velocity for each station pair, and 22 constraints built as follows. The first 10 constraints described the mass conservation for the first 10 layers for the whole section; the next 2 constraints described the mass conservation for layers 11 and 12 for the Caribbean; the next 7 constraints described the mass conservation for layers 11-17 north of Puerto Rico; another constraint (20) described the overall mass conservation for the whole section; constraint 21 was for the overall mass conservation in layers

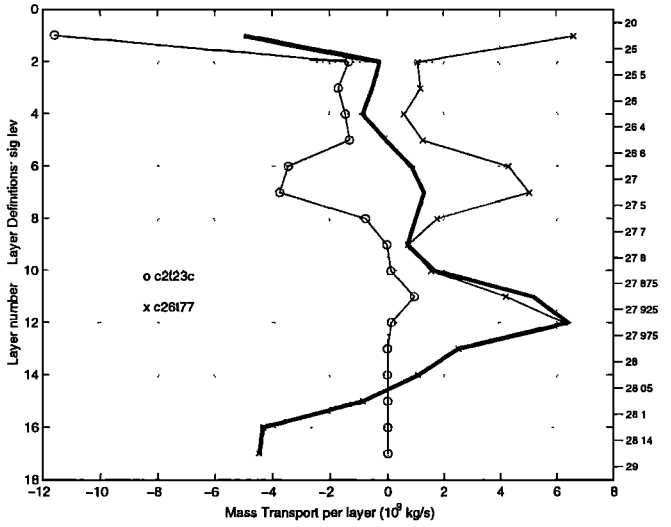

Figure 6. As in Figure 4, but using the geostrophic flow adjusted to the LADCP data.

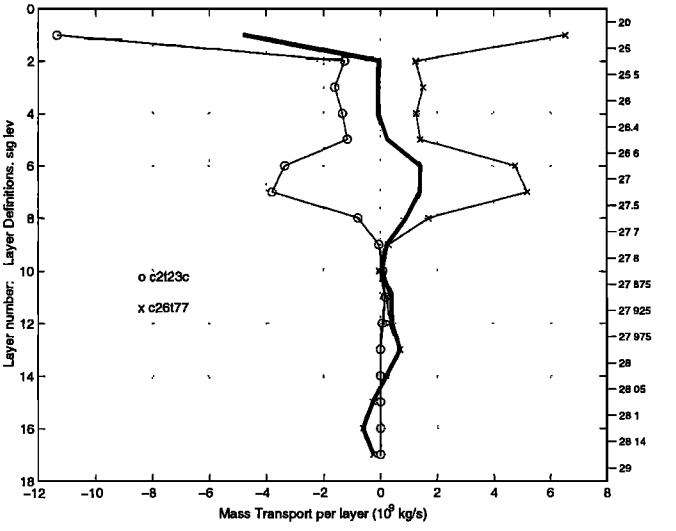

Figure 7. As in Figures 4 and 6 but using the geostrophic flow adjusted to the LADCP data and the solution of the inverse model considering mass conservation.

11-12 for the Caribbean; and the last constraint (22) was for the deep mass conservation for layers 11-17 north of Puerto Rico. We have had to separate the mass conservation equations for deeper layers in the Caribbean from those north of Puerto Rico because the Caribbean is a closed basin from layer 11 downward. These 22 constraints were assigned different a priori estimates of error in the solution of the inverse problem using the Gauss-Markov method [*Wunsch*, 1996]. This method requires a preliminary variance for each velocity and for each constraint. For the a priori velocity variance we have considered the same value for all station pairs with LADCP measurements and a higher value for the rest. They were $(0.05 \text{ m s}^{-1})^2$ and $(0.1 \text{ m s}^{-1})^2$, respectively. For the a priori variance for each constraint we chose higher values in surface layers than in deeper layers, and these last values were higher than the three different overall constraints. Specifically, we chose a value of $(2 \text{ Sv})^2$ for the first four layers, $(0.5 \text{ Sv})^2$ for the last three constraints, and $(1 \text{ Sv})^2$ for the rest of the constraints. By requiring the solution to "balance" to within these limits we are limiting the amount of water mass conversion in the "box," since inflowing water may be converted to outflowing water with a different density. We will see, however, that this aspect of the circulation is very robust and survives despite the contraints put on it.

After the inverse calculation we used the new reference velocities to calculate new mass, salt, and nutrient transports. Figure 7 shows the meridionally integrated mass flux as a function of density layer considering the velocity from the inverse modeling. If we compare Figure 7 and Figure 6, we observe an improvement in the mass conservation for each layer, especially in deep and bottom layers. Nonetheless, there is still an imbalance in specific layers, and we therefore considered using more constraints.

5.4. Silica Constraints and Final Reference Estimates

In order to improve our results we considered using nitrate and silica fluxes as constraints in our inverse model. Figure 8 shows the meridionally integrated nitrate flux as a function of density layer after the inverse calculation using mass constraint. The pattern of the nitrate flux imbalance is very

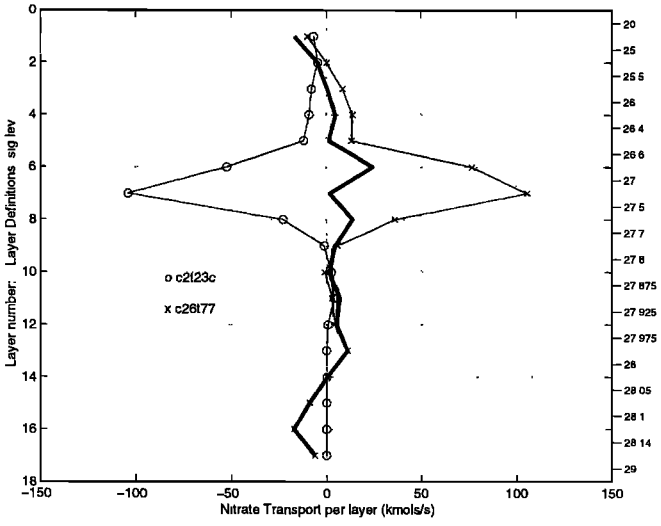

Figure 8. As in Figure 7 but for nitrate flux.

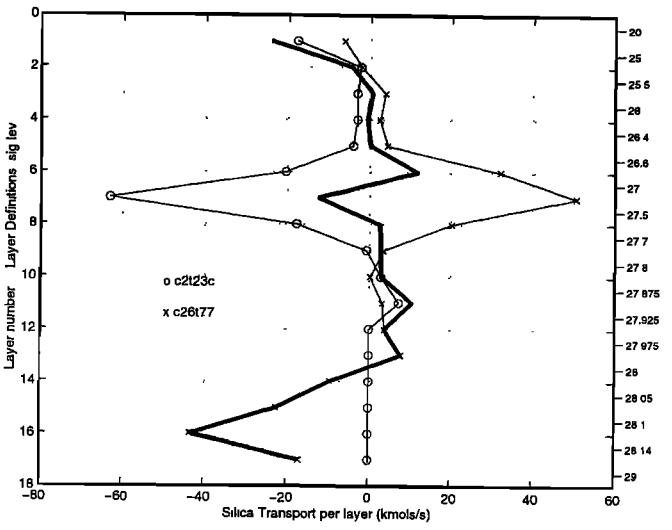

Figure 9. As in Figure 8 but for silica flux.

similar to the pattern of the mass flux imbalance (Figure 8). Thus nitrate flux was not considered as a new constraint in our model because it was not significantly different from mass conservation.

However, silica flux (Figure 9) shows a very different pattern compared to the mass flux pattern (Figure 7), especially in the deep and bottom layers. We therefore considered the silica fluxes as new constraints in our inverse calculations. In addition to our 22 mass constraint equations, we have now added 22 new constraints. The a priori variances for these new equations are $(20 \text{ kmol s}^{-1})^2$ for the first four layers, $(5 \text{ kmol s}^{-1})^2$ for the last three constraints, and $(10 \text{ kmol s}^{-1})^2$ for the rest of the equations. These represent, in part, the degree to which silica is not conserved because of water column dissolution from surface sources and resuspension from bottom sediments. We have chosen a pattern for the a priori variance for silica constraints similar to the one for the mass constraints.

Figure 10a shows the reference velocity adjustment to the initial LADCP-based solution with the error bars as a function of latitude determined by the inverse calculation using mass and silica constraints. In Figure 10a, we observe that the values are negative in the southern half of the Caribbean and positive in the northern half. The results of the inverse calculation attempt to slow down the cyclonic gyre occurring in the deep Caribbean. North of Puerto Rico, the magnitude of the westward flow between 23°-27°N has been increased, while the eastward flow of the deep water in and immediately north of the Puerto Rico Trench is increased. These two changes eliminate much of the deep silica imbalance (Figure 9). In all cases the magnitude of the reference velocity change is < 1 cm s^{-1} compared to that with mass flux constraints alone.

In order to calculate new mass, heat, salt, and nutrient transports we have to add the velocity values obtained from the inverse modeling to the LADCP adjusted velocities as observed in Figure 10b. Here we can see the degree to which the velocities from the inverse calculation slightly modify the LADCP adjusted velocities. In general, our major new information about the reference flow comes from the LADCP, with the inverse results adding some final adjustments. We

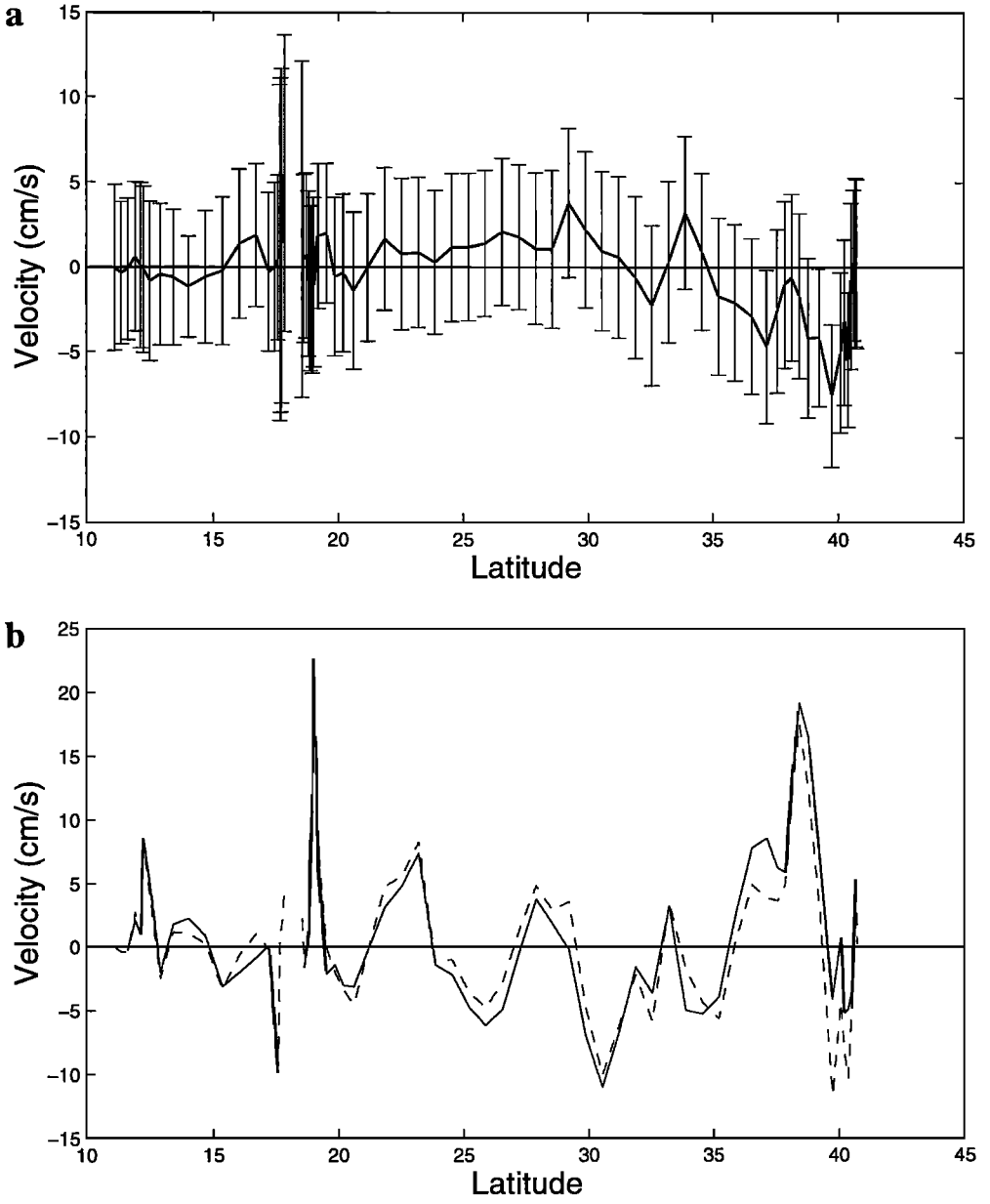

Figure 10. (a) Velocity values as function of latitude line determined by inverse calculations using mass and silica constraints. The error bar for each value is also shown. (b) LADCP adjusted velocities as a function of latitude (solid line) and LADCP adjusted velocities plus velocities determined by inverse calculations using mass and silica constraints (dashed).

can see from Figure 10 that the reference flow in the DWBC to the north of the Gulf Stream has been made more negative while that within the Gulf Stream has been reduced from the LADCP-only case.

The "final" meridionally integrated mass transport (Figure 11) as a function of density layer should be compared to previous ones (Figures 4, 6, and 7) to observe the evolution of this metric of the circulation using different approaches. The remaining imbalances proved robust and will be discussed in section 7.

6. Adjusted Zonal Circulation

The adjusted geostrophic circulation obtained by the inverse procedure (Figure 12) displays many of the same features as in Figure 2b, although smoothing of station pairs is used instead of data at individual stations. The general details of the flow have already been discussed using the LADCP data and will not be reproduced here. Instead, we will discuss the vertically integrated flow between different density surfaces starting with the total (Figure 13) and layer-averaged (Figure 14) mass transport stream functions. As our integration starts to the south, we begin our discussion there. With the exception of the coastal flow north of Venezuela, flow in the upper layers of the Caribbean is everywhere westward, with no indication of the alternating bands of eastward flow seen by *Morrison* [1990] at the Aves Ridge. The net westward flow across the Caribbean is -24 Sv, of which a mere 0.2 Sv is in the Ekman layer. This is a slight increase over what we obtained initially (Figure 7), but the difference is small and indicates how robust the net flow estimate is. So it is not surprising that our result differs little

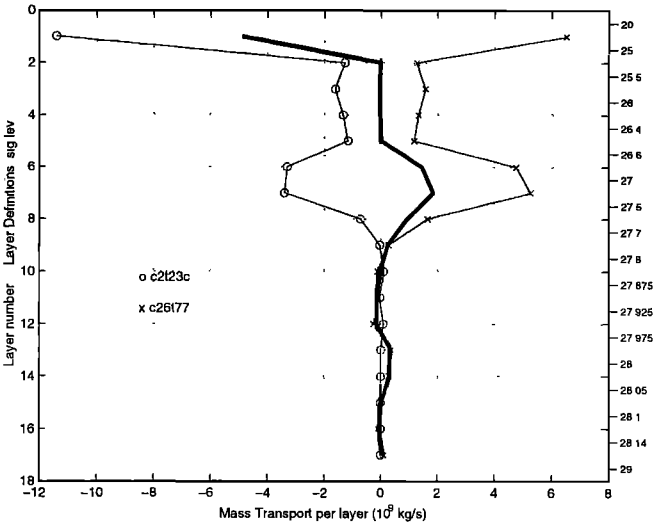

Figure 11. As in Figure 7 but using the solution of the inverse model considering mass and silica constraints.

from that of *Roemmich* [1981], who obtained -22 Sv for water with temperatures < 7°C; *Morrison and Nowlin* [1982], who obtained a total transport of -26 Sv in the Venezuelan Basin; and *Gordon* [1967] who estimated a transport of -29 Sv for the eastern Caribbean. North of Puerto Rico, there is a greater contrast between the two transport stream function estimates (Figures 5 and 13). We defer discussing the reversals in the flow from Puerto Rico northward to about 29N until later in this section. Between 29°N and about 36°N, an energetic westward recirculation is seen south of the Gulf Stream. This is a region of relatively high oxygen and CFCs from northern source waters. Within the Gulf Stream the transport increases and we observe between 153 and158 Sv of eastward transport at this longitude; the range in estimate comes from different station pairs chosen for the "edge" of the flow. *Johns et al.* [1995, Figure 13] show that the major downstream transport increase of the Gulf Stream has occurred by 66°W and that the long-term mean at this longitude should be 140-150 Sv. To the north of the stream there is a net westward flow of -38 to -42 Sv in the northern recirculation gyre [*Hogg et al.* 1986], which compares with -40.4 Sv from Johns et al. at 68°W and *Hogg et al.* 1996 for the 60°-65°W region. Thus our synoptic Gulf Stream appears to be transporting somewhat more water eastward than expected from a long-term mean with about the same amount westward north of the Gulf Stream as the long-term mean near this longitude.

We have divided the water column up into 17 layers for our analysis, but here we group our results into 6 layers showing the vertical structure of the zonal mass transport at 66°W (Figure 14). Given the errors in the inverse solution, one should not expect the streamfunctions of individual or groups of layers to be determined correctly to within ±1 Sv. As above, we begin in the Caribbean and point out that the deep flow in layers 10-11 (layer 12 does not exist in the Caribbean) shows a cyclonic gyre with a maximum mass transport of 15 Sv. This arises principally from the eastward boundary current on the southern side of the basin and the westward flow on the northern flank. This is the first direct observation of an energetic deep cyclonic flow in the Caribbean, although *Roemmich* [1981] suggested that a deep cyclonic flow existed in the Venezuelan Basin on the basis of IGY data and his inverse solution. However, those data did not resolve flow at the boundary because of coarse station spacing, nor were direct velocity estimates available.

To the north of Puerto Rico, the DWBC is observed to have a tight cyclonic recirculation over the trench, with eastward flow of high oxygen and high-CFC waters up to about 23°N. At this point the net transport of the LSW layer is ~11.5 Sv, with the two deeper levels reaching values of 16 and 16.5 Sv, giving a total eastward transport in the DWBC of 44 Sv, of which 41 Sv consists of the NADW components (excluding Antarctic Bottom Water (AABW)). North of the DWBC, our layer stream functions oscillate with westward flow in the deep water between 23° and 27°N and eastward

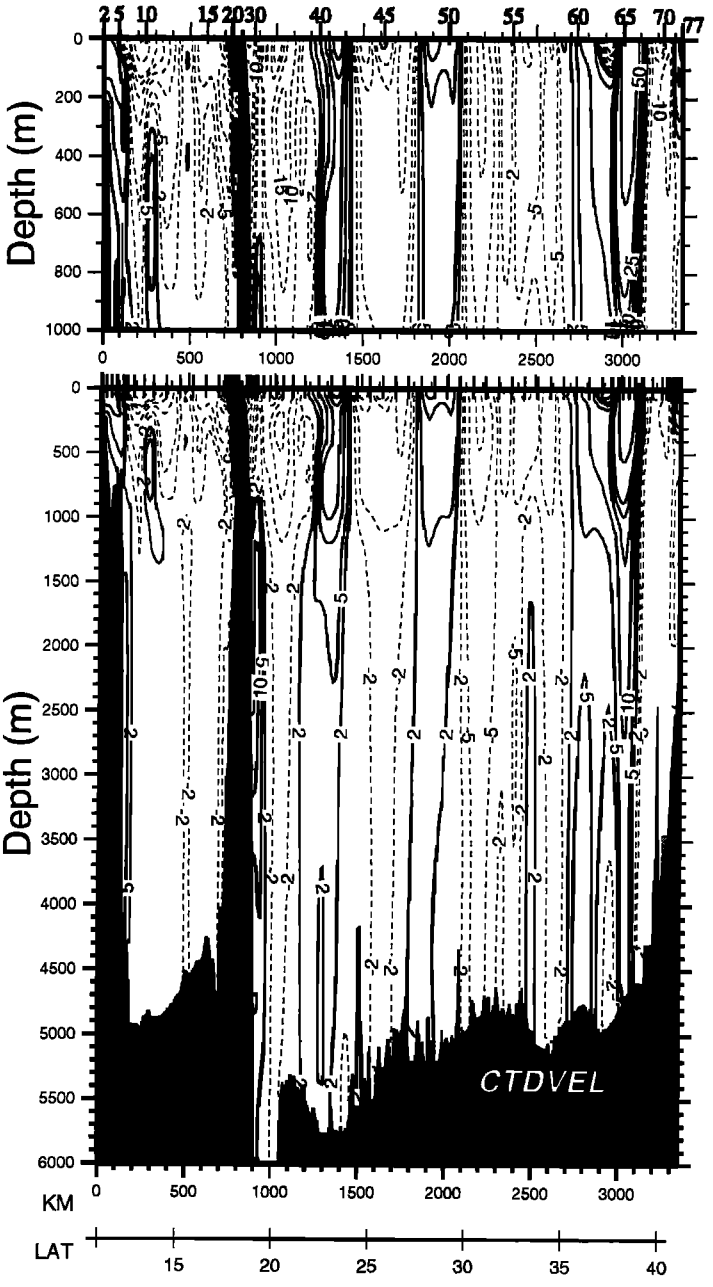

Figure 12. Adjusted geostrophic velocities after the inverse model with mass and silica constraints. These are normal to the section, and the sign convention is the same as in Figure 2b.

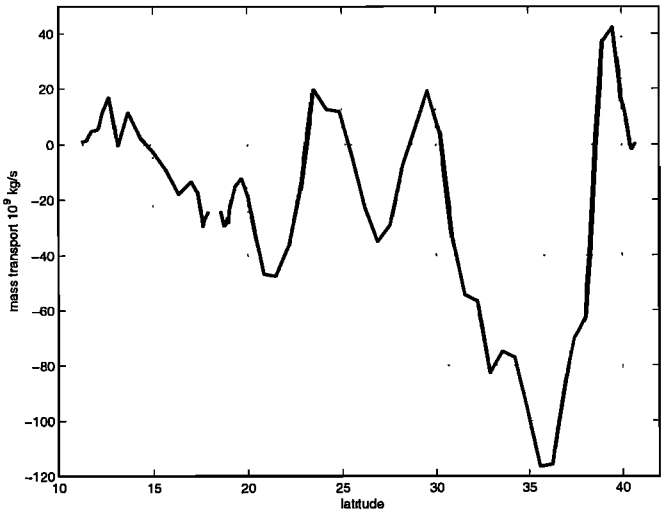

Figure 13. Meridional mass transport stream function for all layers as a function of latitude. As in Figure 5 but using the final adjusted reference velocities from Figure 12.

flow to about 29°N. Were it not for the large water mass contrasts at mid-depths to large depths between these two regimes of flow, one might ascribe them to an eddy. However, the westward flowing portion contains the least ventilated portion of our section, as seen in the higher nutrients, lower oxygen, and lower CFCs. Consistent with our results at 52°W, [manuscript in prepration], 2001, this westward flow appears nearly to be disconnected from the ventilated source waters of the deep boundary currents. We obtain a total westward NADW transport in layers 10-16 of about 25 Sv between 23° and 27°N. These results cannot be compared directly with those of *Schmitz* [1996, Figure I-86] or *McCartney* [1993] because of differences in the definitions of density or potential temperature layers. However, they are in good qualitative agreement in that a strong re-circulation pattern is indicated by both. This will be discussed further later.

To the north of 27°N, we reenter more ventilated water. The eastward flow up to 29°N could be the southern sector of an eddy in the recirculation gyre to the south of the Gulf Stream since the deep water mass contrast is small in the deepest layers between the eastward flow in this latitude band and that immediately to the north. However, this is not the case for the shallower LSW layers, especially for CFCs. Therefore we have not given a definite estimate for the westward recirculation transport of the Gulf Stream since its southern boundary is unclear from our measurements.

Between the northern edge of the Gulf Stream and the boundary, principally the three deep layers carry most of the total westward transport of the northern recirculation gyre/DWBC with -15, -12.5, and -10 Sv in layers 10-12, 13-15, & 16-17, respectively, for a total of -37.5 Sv; since there is no AABW in this region, this transport is all due to North Atlantic Dep Water (NADW) components. It is this region of deep westward flow that introduces the recently ventilated water into the western subtropical North Atlantic.

7. Heat and Freshwater Fluxes

Our inverse solution was one in which no mixing between layers was permitted. Mass balance was sought for each layer within some error bounds. Yet inspection of Figures 4, 6, 7, and 11 will show that there is a net inflow of surface waters into our box and a net outflow of water in layers 6-8. That this is seen in all of the above iterations indicates that it is a robust circulation feature, which survives despite the imposition of the inverse constraints. The light water flowing into the Caribbean at the surface can be cooled by air-sea exchange and become denser. The densest water within our box that undergoes air-sea exchange in winter is the "mode" water of the slope water over the Mid-Atlantic Bight [*Wright and Parker,* 1976]. This water mass is found in winter seaward of the shelf front south of New England. In this region between the shelf and the Gulf Stream, winter cooling of the upper 150 m can produce a water mass with a temperature and salinity range of 10-13°C and 34.8-35.6 psu, respectively. This water flows generally westward and eventually becomes part of the eastward flowing Gulf Stream as part of the northern recirculation region. The neutral density range associated with this water mass includes both layers 7 and 8. Thus the overturning circulation associated with the range of water mass conversion by wintertime air-sea exchange to the west of our section extends from the surface down to layer 8: this is precisely the overturning mode suggested by our net layer transports.

We have used our inverse results to calculate a net heat exchange across our section to be between -0.4 and -0.5 Pw (1 Pw=10^{15} W). For both heat and freshwater we provide a range rather than the mean and 1 standard error. Our section was done during the summer months and we would expect that the above may be an underestimate. In winter the southern waters entering the Caribbean remain warm, but the northern waters leaving the box would be colder, therefore implying a larger heat exchange in winter. A number of zonal lines taken in WOCE (and before) have been used to estimate net heat flux across individual sections [e.g., *MacDonald,* 1998, *Hall and Bryden,* 1982]. These have been compared to meridional heat flux estimates based on integrated annual heat exchange at the ocean surface. The seasonal component of heat flux in the zonal sections has often been neglected or

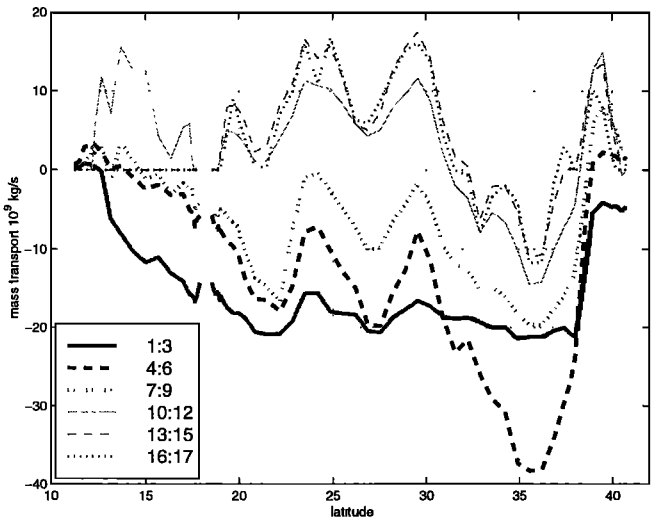

Figure 14. Meridional mass transport stream function for different groups of layers corresponding roughly to near surface (1-3), thermocline (4-6), AAIW (7-9), LSW (10-12), Nordic overflow waters (13-15) Lower Deep Water and Antarctic Bottom Water (16-17).

removed by using a seasonal Ekman transport estimate. As we have noted, the latter is negligible for our section, and in the spirit of the zonal hydrographic lines we compare our heat flux estimate to the *da Silva et al.* [1994] mean annual exchange between 1954 and 1990 from Comprehensive Ocean-Atmosphere Data Set (COADS) integrated over the oceanic region to the west of our section. The total heat loss to the atmosphere in this region is -0.25 Pw, or about -21.7 Wm^{-2}. The two disparate estimates disagree by an amount equivalent to -15 to -25 Wm^{-2}, which is plausibly within the level of the global adjustments in COADS net heat fluxes made by *da Silva et al.* [1994], and the uncertainty estimates of the net COADS heat flux product [c.f. *Josey et al.* 1999].

Freshwater flux is a very important element in climate studies. The knowledge of the divergence of freshwater flux in closed sections could aid in the understanding of the global water cycle and climate. We have followed the study of *Wijffels et al.* [1992] and the procedure of *Wunsch* [1996] even though we know that there is some concern because we are dealing with small numbers within a frame of noisy calculations.

Let T be a matrix with elements T_{ij} equal to the mass transport in layer i at station pair j, including the total velocity field (relative plus reference) and the Ekman component in the first layer. The mass conservation can be written

$$\sum_i \sum_j T_{ij} + n_1 = -F , \quad (2)$$

where F is the excess of evaporation over precipitation plus runoff in the closed volume. Conservation of salt is

$$\sum_i \sum_j T_{ij} S_{ij} + n_2 = 0 . \quad (3)$$

If S_0 is the mean salinity, then $S'_{ij}=S_{ij}-S_0$, and (3) is

$$\sum_i \sum_j T_{ij} (S'_{ij} + S_0) + n_2 = 0 . \quad (4)$$

From (2), $\sum\sum T_{ij}=-F-n_1$, and (4) can be rewritten

$$\sum_i \sum_j T_{ij} S'_{ij} - (F + n_1) S_0 + n_2 = 0 . \quad (5)$$

Thus

$$F = \left(\sum_i \sum_j T_{ij} S'_{ij} - n_1 S_0 + n_2 \right) \Big/ S_0 . \quad (6)$$

Under the assumption $\langle n_1 \rangle = \langle n_2 \rangle = 0$, the best estimate of F is

$$\tilde{F} = \sum_i \sum_j T_{ij} S'_{ij} \Big/ S_0 . \quad (7)$$

For our closed section the freshwater flux estimate is 0.31-0.37 Sv, which indicates that the area to the west of our section must lose a net amount of freshwater (evaporation E minus precipitation P and runoff). This is equivalent to stating that there is a net positive salinity flux out of the region. As in the case of the net heat flux, we have compared our estimate with that derived from the COADS data (*da Silva et al.* 1994), which yields a net E-P of 0.20 Sv. As with the heat flux, it appears that our estimate exceeds that from *da Silva et al.* [1994] by a factor of about 1.5. It is likely that the large amount of low salinity water identified as coming from the Orinoco River and flowing westward in the mid-Caribbean [see *Hernandez-Guerra and Joyce*, 2000] contributes to a seasonal signal that might bias our estimate to be high. *Wijffels et al.* [1992] estimated that the Atlantic Ocean as a whole loses 0.56 Sv of freshwater in net evaporation minus precipitation and runoff to the atmosphere. Our result suggests that a significant fraction of this is lost west of 66°W.

8. Discussion

Within the Caribbean Sea we have observed a deep cyclonic gyre with a transport of 15 Sv. This exceeds by a factor of 100 the deep inflow through the A-J Passage [*MacCready, et al.* 1999] and is difficult to explain by flat bottom source/sink flows of the type discussed by *Stommel and Arons* [1960]. *Johnson* [1998] has presented arguments for deep cyclonic gyres over trenches based on weak inflow at depth and mixing across steep topography. Perhaps this should be considered for the Caribbean as well as over the Puerto Rico trench. The effect of eddy stresses in the basin, as presented in the *Sou, et al.* [1996] study of the Caribbean, might be another mechanism for generating this deep cyclonic flow. The low-silica, high-CFC remnants of deep overflows are still seen on the bottom of the Caribbean both in the north (just downstream of the sill) and to the south near Venezuela, suggesting again that a deep circulation is present connecting the two regions. However, the lack of CFC signals at depths of 2000 m to the south is a puzzle in view of the fact that we see CFCs at this depth to the north near Puerto Rico. One can see from the topography (see 1700 m contour in Figure. 1) that a cyclonic boundary current of about 5 cm s^{-1}, which is similar to what we observe, would advect CFCs around the perimeter distance of ~4000 km in about 2 years. However, in locations where we have been able to estimate spreading rates from CFC and tritium/^{3}He data the spreading rates have been 1-2 cm s^{-1} [*Weiss et al.*, 1985; *Doney and Jenkins*, 1994; *Smethie et al.*, 2000), a factor of 5-10 less than direct current measurements. The reason for this is recirculation and exchange of water between the boundary current and the interior. Thus 10 years might be a more realistic time for the CFC signal to spread around the Caribbean at 1700 m. Since no CFC signature is seen to the south at this level, we might conclude that the CFC signals represent a recent (<10 year) injection of Atlantic water at middepth. The long-term variations of LSW [*Lazier*, 1995] indicate that recent output of CLSW began about 1990 and, though present at the northern end of our section, has not yet reached the A-J inflow in any significant amounts. Thus the bottom CFC maximum in the Caribbean could be an older remnant of CLSW, while the one at middepths could be a recent injection of ULSW that is present in quantity at the A-J Passage. However, both the deep and middepth CFC maxima have similar CFC-11:CFC-12 ratios, suggesting a similar "age" (30-35 years, for the same mixing ratio with ambient water). Consistent with this scenario then, the shallower CFC maximum has a longer transit path around the basin, in contrast with the bottom maximum, which is confined to the Venezuelan Basin and has a much shortened transit path. This would permit a bottom signal to appear to the south before the one at middepth, given that both layers were ventilated at the same time within the past 10 years.

The DWBC north of Puerto Rico has a small-scale flow reversal over the trench before it resumes an eastward course and transports 41 Sv of LSW and LNADW to the east. A region of westward flow between 24° and 27°N is the least ventilated portion of the middepth and deep water on the section and has a transport of -25 Sv. This water is similar in properties to poorly ventilated water on our 52°W section and has a CFC age (derived from the CFC ratio) for the lower tracer core that is 4 years older than the eastward flow near the boundary. The shallow ULSW core in the recirculation seems to have picked up CFCs by mixing with the boundary

flow because it is the same age as the boundary flow and "younger" than in the recirculating flow at 52°W, which conflicts with the hypothetical model of a Guiana recirculation gyre by McCartney (1993) and Schmitz (1996); this will be discussed further in a later paper which deals with the 52W section. Adding together the two vigorous opposing flows, we obtain a net eastward transport of 16 Sv for the deeper limb of the Atlantic thermohaline circulation, excluding AABW. The deep recirculation at 66°W could significantly alter the properties of the DWBC west of our section as it impinges upon the DWBC which is undiluted by the "older," less ventilated water. Evidence to support this would be if the DWBC abruptly changed water mass characteristics and transport along its path consistent with an inflow of higher nutrient, lower CFC, and lower-oxygen waters associated with this westward flow.

The shallow overturning circulation we found has net inflow of near-surface water flowing westward into our closed box within the Caribbean and denser water flowing out of the box at shallow sub thermocline depths mainly in the north. This overturning circulation can be explained in terms of air-sea exchange. Imagine a stack of layers flowing into the box with air-sea cooling removing a fraction of water from each level and adding it to the layer below before it exits. The net result would be that there would be an excess of mass flowing in at the surface and an excess flowing out at the deepest level exposed to the atmosphere in winter. This is what we observe: the mode water of the slope water that is found between the Gulf Stream and the continental shelf south of New England is the densest water at the surface in winter to the west of our section and the deepest layer of our shallow overturning cell (STMW is formed to the east of our section). The implied heat loss to the atmosphere can be calculated to be in the range of -0.4 to -0.5 Pw, which exceeds that expected from COADS net heat losses to the west of our section, although remains plausible given the uncertainty in the estimate of the net heat flux at the ocean surface. One might argue that our net heat flux could be an underestimate because we formally required the net mass transport in each layer to vanish to within some limits, thus minimizing the overturning portion of the circulation and its attendant heat flux. We have also estimated a net freshwater flux of 0.31--0.37 Sv, which again exceeds that expected from the mean difference between evaporation and precipitation to the west of our section from COADS of 0.20 Sv but could point to systematic errors in the climatology of the *E-P* fields.

Finally, we would like to point out the utility of LADCP data in adding information to our circulation. Without these data our circulation (based on geostrophy and inverse constraints) would not have been as energetic in the recirculation zones nor as accurate in resolving boundary current transports, and we would not have seen such clear evidence for a deep cyclonic circulation of the Caribbean. Though some care must be associated when using LADCP data, they seem to have been used sparingly in basin-wide studies of the general circulation thus far.

Acknowledgments. We wish to acknowledge the support of NSF grants OCE95-29607 (T.J.), OCE95-31864 (W.S.) and the support of the Secretaría de Estado de Universidades, Investigación y Desarrollo (A. H.-G.). We further thank Jane Dunworth-Baker for her assistance with the plotting and calculations, Paul Robbins for use of his MATLAB scripts, Alex Ganachaud for discussions about inverse methods, Frank Bahr for his attention to the LADCP data and processing, and our seagoing WOCE colleagues for such a fine data set with which to work. We also thank Mindy Hall and two anonymous reviewers for their comments on an earlier draft of this manuscript. This is contribution number 10153 of the Woods Hole Oceanographic Institution and number 6166 from Lamont-Doherty Earth Observatory.

References

da Silva, A. M., and S. Levitus (eds.), 1994. Atlas of marine data 1994, volume 1: algorithms and procedures, 83 pp., U.S. Dept. of Commerce, December 1994.

Doney, S. C., and W. J. Jenkins, Ventilation of the Deep Western Boundary Current and Abyssal Western North Atlantic: Estimates from tritium and ^{3}He distributions, *J. Phys. Oceanogr., 24,* 638-659, 1994.

Firing, E. and L. Gordon, Deep ocean acoustic Doppler profiling, paper presented at *Fourth Working Conference on Current Measurements*, Inst. of Electr. And Elct. Eng., Clinton MD. August 1990.

Fischer, J. and M. Visbeck, Deep profiling with self-contained ADCPs, *J. Atmos. Oceanic Technol., 10,* 764-773, 1993.

Fratantoni, D. M., R. J. Zantopp, W. R. Johns, and J. L. Miller, Updated bathymetry of the Anegada-Jungfern Passage complex and implications for Atlantic inflow to the abyssal Caribbean Sea, *J. Mar. Res., 55,* 847-860, 1997.

Gordon, A. L., Circulation of the Caribbean Sea, *J. Geophys. Res., 72,* 6207-6223, 1967.

Hall, M. M., and H. L. Bryden, Direct estimates and mechanisms of ocean heat transport, *Deep Sea Res., Part A, 29,* 339-359, 1982.

Hernandez-Guerra, A., and T. M. Joyce, Water masses and circulation in the surface layers of the Caribbean at 66°W, *Geophys. Res. Lett., 27,* 3497-3500, 2000.

Hogg, N. G., R. S. Pickart, R. M. Hendry, and W. J. Smethie, The northern recirculation gyre of the Gulf Stream, *Deep Sea Res., Part A, 33,* 1139-1165, 1986.

Jackett, D., and T. J. MacDougall, A neutral density variable for the world's ocean, *J. Phys. Oceanogr., 96,* 237-263, 1996.

Johns, W. E., T. J. Shay, J. M. Bane, and D. R. Watts, Gulf Stream structure, transport, and recirculation near 68°W, *J. Geophys. Res., 100,* 817-838, 1995.

Johnson, G. C., Deep water properties, velocities, and dynamics over ocean trenches, *J. Mar. Res., 56,* 329-347, 1998.

Josey, S. A., E. C. Kent, and P. K. Taylor, New insights into the ocean heat budget closure problem from an analysis of the SOC air-sea flux climatology, *J. Clim., 12,* 2856-2880, 1999.

Joyce, T. M., WOCE operations manual, rev. 1, WHP Off. Rep. *WHPO 91-1, WOCE Rep. 68/91,* November 1994, revision 1, Woods Hole, Mass, USA, 1994.

Joyce, T. M., and P. Robbins, The long-term hydrographic record at Bermuda, *J. Clim., 9,* 3121-3131, 1996.

Joyce, T. M., R. S. Pickart, and R. C. Millard, Long-term hydrographic changes at 52 and 66°W in the North Atlantic subtropical gyre and Caribbean, *Deep Sea Res., Part II, 46,* 245-278, 1999.

Knapp, G. P., 1988. Hydrographic data from R. V. Endeavor cruise 129. Woods Hole Oceanographic Inst. Technical Report 88-41, Sept. 1988, 111 pp.

Lazier, J. R. N., The salinity decrease in the Labrador Sea over the past thirty years, in Natural Climate Variability on Decade-to-Century Time Scales, edited by D. G. Martinson, et al., pp. 295-304, Nat. Res. Counc., Nat. Acad. Press, Washington, D.C., 1995.

MacCready, P., W. E. Johns, C. G. Rooth, D. M. Fratantoni, and R. A. Watlington, Overflow into the deep Caribbean: Effects of plume variability, *J. Geophys. Res., 104,* 25,913-25,935, 1999.

MacDonald, A. M., The global ocean circulation: a hydrographic estimate and regional analysis, *Prog. Oceanogr., 41,* 281-382, 1998.

McCartney, M. S., Recirculating components to the deep boundary current of the northern North Atlantic, *Prog. Oceanogr., 29,* 283-383, 1992.

McCartney, M. S., Crossing of the equator by the Deep Western Boundary Current in the western Atlantic Ocean, *J. Phys. Oceanogr., 23,* 1953-1974, 1993.

Metcalf, W. G., Caribbean-Atlantic exchange through the Anegada-Jungfern Passage. *J. Geophys. Res. 81,* 6401-6409,

Morrison, J. M., Geostrophic transport variability along the Aves Ridge in the eastern Caribbean during 1985-1986, *J. Geophys. Res., 95,* 699-710, 1990.

Morrison, J. M., and W. D. Nowlin, General distribution of water masses within the eastern Caribbean Sea during the winter of 1992 and the fall of 1973, *J. Geophys. Res., 87,* 4207-4229, 1982.

Pickart, R. S., Water mass components of the North Atlantic Deep Western Boundary Current, *Deep Sea Res., Part A, 39,* 1553-1572, 1992.

Pickart, R. S. and W. M. Smethie, Jr., Temporal evolution of the Deep Western Boundary Current where it enters the sub-tropical domain, *Deep Sea Res. Part I, 45,* 1053-1983, 1998.

Price, J. F. and M. O. Baringer, Outflows and deep water production by marginal seas, *Prog. In Oceanogr., 33,* 161-200, 1994.,

Roemmich, D., Circulation of the Caribbean Sea: A well-resolved inverse problem, *J. Geophys. Res., 86,* 7993-8005, 1981.

Schmitz, W. J. Jr., On the world ocean circulation: vol. I, *Woods Hole Oceanogr. Inst. Tech. Rep.* 96-03, 141 pp, Woods Hole, Mass., 1996.

Smethie, W. M., 1993. Tracing the thermohaline circulation in the western North Atlantic using chlorfluorcarbons. *Prog Oceanogr.*, 31, 51-99.

Smethie, W. M., Jr., R. A. Fine, A. Putzka, and E. P. Jones, Tracing the flow of North Atlantic Deep Water using chlorofluorocarbons, *J. Geophys. Res., 105,* 14,297-14,323, 2000.

Sou, T., G. Holloway, and M. Eby, Effects of topographic stress on the Caribbean Sea circulation, *J. Geophys. Res., 101,* 16,449-16,453, 1996.

Stalcup, M. C. and W. G. Metcalf, Bathymetry of the sills for the Venezuela and Virgin Islands basins. *Deep Sea Res., Oceanog. Abstr. 20,* 739-742. 1973.

Stalcup, M. C., W. G. Metcalf, R. G. Johnson, Deep Caribbean inflow through the Anegada-Jungfern Passage. *J. Mar. Res., 33,* Suppl., 15-35, 1975.

Stommel, H. and A. B. Arons, On the abyssal circulation of the world ocean, II, An idealized model of the circulation pattern and ampplitude in ocean basins, *Deep Sea Res., 6,* 217-233, 1960.

Weiss, R. F., J. L. Bullster, R. H. Gamon, and . J. Warner, Atmospheric chlorofluoromethanes in the deep equatorial Atlantic, *Nature, 314,* 608-610, 1985.

Wijffels, S. E., R. W. Schmitt, H. L. Bryden, and A. Stigebrandt, Transport of freshwater by the oceans, *J. Phys. Oceanog., 22,* 155-162, 1992.

World Ocean Circulation Experiment [WOCE], Mean surface wind fields from the ERS-AMI and ADEOS-NSCAT microwave scatterometers, paper presented at WOCE Conference, Halifax, Canada, May 1998.

Worthington, L. V., The 18°C water in the Sargasso Sea, *Deep Sea Res., 5,* 297-305, 1959.

Wright, W. R. and C. E. Parker, A volumetric temperature/salinity census for the Middle Atlantic Bight, *Limnol. and Oceanogr., 21,* 563-571, 1976.

Wunsch, C., The North Atlantic general circulation west of 50°W determined by inverse methods, *Rev. Geophys., 16,* 583-620, 1978.

Wunsch, C., *The Ocean Circulation Inverse Problem,* 442 pp., Cambridge Univ. Press, New York, 1996.

Wüst, G., *Stratification and Circulation in the Antillean-Caribbean Basins,* 201 pp. Columbia Univ. Press, New York, 201 pp, 1964.

Alonso Hernandez-Guerra, Universidad de Las Palmas de Gran Canaria, Departamento de Fisica, Campus Universitario De Tafira, 35017, Las Palmas, GC, Spain

T. M. Joyce, Woods Hole Oceanographic Institution, Department of Physical Oceanography, MS #21, Woods Hole, MA 02543

W. M. Smethie, Jr., Lamont Dohery Earth Observatory, P.O. Box 100, 61 Route 9W, Palisades, NY 10964

(Received February 9, 2000; revised March 5, 2001; accepted March 26, 2001.)